

See discussions, stats, and author profiles for this publication at: <https://www.researchgate.net/publication/280059847>

Adsorption and Reaction of C₂H₄ and O₂ on Nano-sized Gold Cluster: A Computational Study

ARTICLE *in* THE JOURNAL OF PHYSICAL CHEMISTRY A · JULY 2015

Impact Factor: 2.69 · DOI: 10.1021/acs.jpca.5b04737 · Source: PubMed

READS

29

2 AUTHORS, INCLUDING:



Hsin-Tsung Chen

Chung Yuan Christian University

78 PUBLICATIONS 704 CITATIONS

[SEE PROFILE](#)

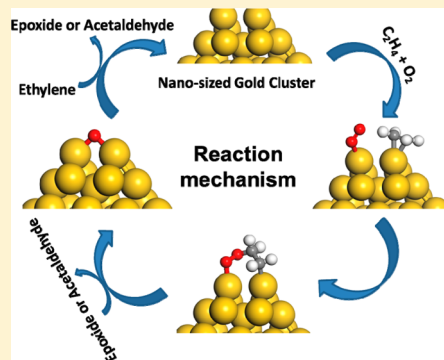
Adsorption and Reaction of C_2H_4 and O_2 on a Nanosized Gold Cluster: A Computational Study

Chen-Chi Lee and Hsin-Tsung Chen*

Department of Chemistry, Chung Yuan Christian University, Chungli District, Taoyuan City 32023, Taiwan

Supporting Information

ABSTRACT: We have investigated the adsorption and reaction mechanisms of C_2H_4 and O_2 catalyzed by a Au_{38} nanoparticle based on periodic density-functional theory (DFT) calculations. The configurations of the adsorption of C_2H_4/Au_{38} , O_2/Au_{38} , and O/Au_{38} as well as the coadsorption of $C_2H_4-O_2/Au_{38}$ were predicted. The calculation results show that C_2H_4 , O_2 , and O are preferably bound at top (T), bridge (B), and hexagonal (h) sites with adsorption energies of -0.66 , -0.99 , and -3.93 eV, respectively. The detailed reaction mechanisms for ethylene epoxidation on the Au_{38} nanoparticle has been illustrated using the nudged elastic band (NEB) method. The oxidation process takes place via the Langmuir–Hinshelwood (LH) mechanism to generate ethylene oxide and acetaldehyde. The overall reaction of $C_2H_4 + O_2 + Au_{38} \rightarrow$ ethylene oxide + O/Au_{38} is exothermic by 2.20 – 2.40 eV whereas those are 3.03 – 3.08 eV for the production of acetaldehyde and O/Au_{38} . The nature of the interaction between the adsorbate and gold nanocluster has been analyzed by the detailed electronic local density of states (LDOS) to understand the high catalytic activity of the gold nanoclusters.



INTRODUCTION

The epoxidation of alkene is a practical heterogeneous catalytic process in chemical synthesis because epoxide products are essential intermediates for synthesis. It has been demonstrated that nanogold particles are active in variable catalytic reactions, for example, CO oxidation,^{1–3} selective oxidation of alkene and alcohol,^{4,5} the water–gas shift reaction,^{6,7} and hydrogen peroxide synthesis,^{5,8} although the gold metal is originally inactive. Nanogold clusters have recently received a great deal of interest because of their unique and unexpected catalytic property difference from bulk gold.^{9–13} Numerous experimental studies on CO oxidation^{14–17} have shown that nanogold clusters on various metal oxide supports including reducible and nonreducible oxides can promote the reaction at lower temperature or even below room temperature compared to the conventional catalysts, suggesting that these oxides may play an important role in the catalytic reactions.^{9,18–25} The reducible-oxide-supported Au nanocluster provides better reactivity than the nonreducible counterparts owing to the defect effect of reducible oxides. In addition, computational studies have demonstrated that the nanogold clusters can be very catalytic in the CO oxidation reaction.^{1,3,26–33} Patial et al.^{34,35} and Haruta et al.³⁶ also reported that the supported nanogold clusters are active and selective for the propylene and styrene epoxidation. The size and shape of nanogold clusters and the properties of the support oxide lead to the remarkable catalytic properties which might in part come from the strong electronic interactions in the nanogold/oxide catalysts. However, the understanding of the reaction mechanisms of alkene epoxidation is lacking compared to the well-investigated CO

oxidation. Interestingly, Turner et al.¹² showed that nanogold particles (smaller than 1.5 nm) exhibit highly efficient and robust catalytic activity for selective oxidation by the only oxidant, O_2 . The enhanced activity is not yet fully understood. It is therefore of importance to elucidate the detailed catalytic mechanisms of alkene oxidation.

A few theoretical investigations were carried out to make the density-functional theory (DFT) calculations to study the reaction mechanisms of styrene epoxidation on gold nanoparticles.^{27,37–39} Go et al. have shown that the Au_{38} nanocluster is the size threshold for the styrene epoxidation as concerns the adsorption, electronic structure, and activation energy barriers.²⁷ Lyalin et al.⁴⁰ have reported the adsorption of C_2H_4 and O_2 and its cooperative adsorption on small Au_N clusters ($N = 1$ – 10) by DFT calculations because the cooperative adsorption of C_2H_4 and O_2 is particularly vital for understanding the mechanism of alkene oxidation. Chen et al.³⁹ have investigated ethylene oxidation on the Au_{29} cluster by atomic oxygen. However, the detailed mechanisms for C_2H_4 with the O_2 reaction on the nanogold cluster are not clear. In this work, we applied periodic density-functional calculations to investigate the interaction and the detailed mechanisms of the C_2H_4 with O_2 reaction on the Au_{38} cluster to understand the factors influencing the alkene oxidation catalyzed by nanometer-sized gold particles.

Received: May 19, 2015

Revised: July 13, 2015

Published: July 13, 2015

COMPUTATIONAL METHOD

All geometric calculations for the adsorption and reaction of C₂H₄ and O₂ on nanogold clusters were performed with periodic density-functional theory (DFT)⁴¹ at the plane-wave basis set with a spin-polarized effect, as implemented in the Vienna ab initio simulation package (VASP) program^{42–46} with the projector augmented wave (PAW). The interaction between core and valence electrons was described by the generalized gradient approximation (GGA)⁴⁷ with the PW91 functional.⁴⁸ The cell size effect was tested by C₂H₄ adsorption on Au₃₈ with the most stable structure in 20 × 20 × 20, 25 × 25 × 25, and 30 × 30 × 30 Å³ cubic boxes, respectively. The results showed that the 25 × 25 × 25 Å³ cubic supercell is big enough to avoid the possible interaction between the Au₃₈ cluster and its periodic images. A cutoff energy of 400 eV, which permits convergence to 1 × 10⁻⁴ eV in total energy, was chosen. The Brillouin zone with the Γ point was used for the calculations. In this study, we calculated the adsorption energies according to

$$\Delta E_{\text{ads}} = E_{\text{total}} - E_{\text{Au}_{38}} - E_{\text{adsorbate}} \quad (1)$$

where E_{total} , $E_{\text{Au}_{38}}$, and $E_{\text{adsorbate}}$ represent the electronic energies of adsorbed species on the Au₃₈ nanocluster, the bare Au₃₈ nanocluster, and the gas-phase adsorbate, respectively. In addition, the coadsorption energies of C₂H₄ with O₂ species were computed as

$$\Delta E_{\text{coads}} = E_{\text{total}} - E_{\text{Au}_{38}} - E_{\text{C}_2\text{H}_4} - E_{\text{O}_2} \quad (2)$$

The minimum-energy paths (MEP) including reactants, intermediates, and products were illustrated by using the nudged elastic band (NEB) method.^{49,50}

RESULT AND DISCUSSION

As previous studies for the Au₃₈ cluster,^{7,28} the O_h -symmetric tetrakaidecahedral structure with six equivalent square fcc(100)-like faces and eight equivalent hexagonal fcc(111)-like faces is chosen. The predicted average Au–Au bond distance is 2.77 Å, which is consistent with the experimental value of 2.78 Å.⁵¹ As depicted in Figure 1, the C₂H₄, O₂, and O

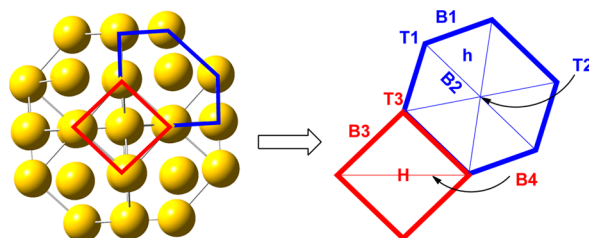


Figure 1. Schematic presentation for various adsorption sites on the hexagonal fcc(111)-like face and square fcc(100)-like face of the Au₃₈ nanocluster. T₁, T₂, and T₃ represent the top sites; B₁, B₂, B₃, and B₄ represent the bridge sites; H represents the hole site; and h represents the hcp site.

species can be placed on several adsorption sites of the Au₃₈ nanocluster which are considered and characterized as top, T (on one Au atom); bridge, B (on the Au–Au bond); hollow, H (on the center of the square fcc(100)-like faces); and hcp, h (on the center of the trigonal plane of the hexagonal fcc(111)-like faces) sites of the nanocluster. Numbers 1, 2, 3, and 4 in

Figure 1 denote different Au atoms or Au–Au bonds of the nanocluster.

Adsorption of C₂H₄, O₂, and O and Coadsorption of C₂H₄ and O₂ on the Au₃₈ Nanocluster. To locate plausible stable adsorption structures of intermediates for the C₂H₄–Au₃₈, O₂–Au₃₈, and O–Au₃₈ interactions, the C₂H₄, O₂, and O species were placed at various sites on the Au₃₈ nanocluster as depicted in Figure 1. The stable optimized structures of the C₂H₄–Au₃₈, O₂–Au₃₈, and O–Au₃₈ interactions are displayed in Figures 2–4, respectively. Their corresponding adsorption energies are summarized in Tables 1–3, respectively. Others corresponding to physisorption (weak adsorption) are depicted in Figures S1 and S2 of the Supporting Information. The C₂H₄–Au₃₈ interactions result in several isomeric configurations according to the various adsorption sites as expected (Figure 2). The C₂H₄ molecule prefers the “side-on” configurations via both C atoms binding to the Au–Au bond (C₂H₄–B₃–μ², see Figure 2) of the square fcc(100)-like faces with an adsorption energy of −0.65 eV. The C₂H₄–T₃–η² structure via two C atoms binding to the same Au atom of the square fcc(100)-like faces with an adsorption energy of −0.62 eV is the second stable one. The C₂H₄–T₁–η² configuration via two C atoms binding to the same Au atom with an adsorption energy of −0.66 eV is energetically the most stable among all of the calculated C₂H₄–Au₃₈ adsorptions of the hexagonal fcc(111)-like faces. The C₂H₄–B₁–μ² structure via two C atoms binding to the Au–Au bond of the hexagonal fcc(111)-like faces with an adsorption energy of −0.53 eV is the second most stable one. The calculated C–C bonds in the π-bonded C₂H₄–T₁–η² and C₂H₄–T₃–η² structures are lengthened to 1.381 and 1.382 Å compared to that (1.330 Å) of a calculated gas-phase C₂H₄. For the di-σ-bonded C₂H₄ in C₂H₄–B₃–μ² and C₂H₄–B₁–μ² configurations, the calculated C–C bonds are 1.472 and 1.478 Å. As listed in Table S1 (Supporting Information), we assumed that those with the calculated adsorption energies within −0.15–0.05 eV are assigned to weakly bound intermediates (Figure S1). The adsorption behaviors for strongly bound species are similar to their counterparts in small Au_N clusters ($N = 1$ –10) reported by Lyalin et al.^{40,52} For the O₂–Au₃₈ adsorption, six and five stable configurations on the square fcc(100)-like face and hexagonal fcc(111)-like face were found as shown in Figure 3. Table 2 displays the corresponding adsorption energies. The most stable structures of the O₂–Au₃₈ adsorption are located at B₃ and B₄ sites of the square fcc(100)-like face forming O₂–B₃–μ² and O₂–B₄–μ² structures as shown in Figure 3. Their calculated adsorption energies are −0.99 and −0.96 eV, and the O–O bonds are computed to be 1.358 and 1.450 Å, respectively. The O₂–B₁–μ² and O₂–B₂–μ² structures adsorbed at B₁ and B₂ sites of the hexagonal fcc(111)-like face with adsorption energies of −0.98 and −0.74 eV and O–O lengths of 1.366 and 1.359 Å are energetically the two most stable ones. As shown in Table S2 and Figure S2, others are characterized as physisorbed states because of the small adsorption energies. One should note that the adsorption energies of the O₂ molecule are much larger than those of the C₂H₄ molecule. In addition, the Au₃₈ nanocluster possesses a better ability to bind the O₂ molecule ($E_{\text{ads}} = -0.74$ to -0.99 eV) compared to the adsorption energies of O₂/Au (111), O₂/Au (211), and O₂/Au₂₉ constructions ($E_{\text{ads}} \approx 0$ eV for Au (111), $E_{\text{ads}} = -0.15$ eV for Au (211), and $E_{\text{ads}} = -0.60$ eV for Au₂₉). For the O–Au₃₈ adsorption as depicted in Figure 4, the radical adsorbates of O adsorb strongly onto the Au₃₈ nanocluster as expected. The

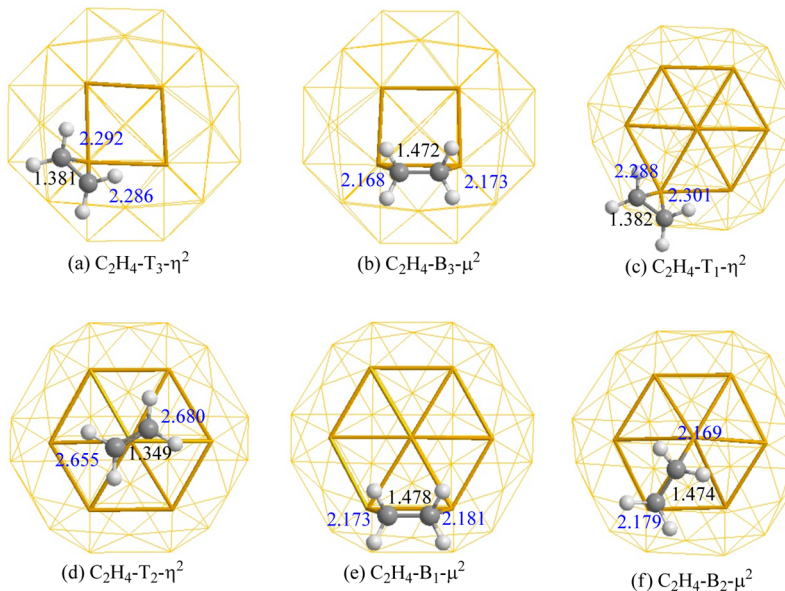


Figure 2. Optimized isomers of adsorbed C_2H_4 on the Au_{38} nanocluster and their important geometric parameters computed at the PW91 level of theory. The bond lengths are given in angstroms.

Table 1. Calculated Adsorption Energies (eV) and Geometrical Parameters (\AA) of Adsorbed C_2H_4 on the Au_{38} Nanocluster

species	E_{ads} (eV)	$d_{\text{Au1-C1}}(\text{\AA})$	$d_{\text{C1-C2}}(\text{\AA})$	$d_{\text{C2-Au2}}(\text{\AA})$
$\text{C}_2\text{H}_4\text{-T}_3\text{-}\eta^2$	-0.62	2.292	1.381	2.286
$\text{C}_2\text{H}_4\text{-B}_3\text{-}\mu^2$	-0.65	2.168	1.472	2.173
$\text{C}_2\text{H}_4\text{-T}_1\text{-}\eta^2$	-0.66	2.288	1.382	2.301
$\text{C}_2\text{H}_4\text{-T}_2\text{-}\eta^2$	-0.28	2.655	1.349	2.680
$\text{C}_2\text{H}_4\text{-B}_1\text{-}\mu^2$	-0.53	2.173	1.478	2.181
$\text{C}_2\text{H}_4\text{-B}_2\text{-}\mu^2$	-0.49	2.179	1.474	2.169

adsorption energies for all of the $\text{O}-\text{Au}_{38}$ structures range between -2.75 and -3.93 eV as listed in **Table 2**. The $\text{O}-\text{h}^3$ structure with an adsorption energy of -3.93 eV, calculated $\text{O}-\text{Au}$ bond lengths of 2.156, 2.160, and 2.149 Å on the hexagonal fcc(111)-like face and the $\text{O}-\text{B}_3\text{-}\mu^1$ structure with an adsorption energy of -3.72 eV, and the calculated $\text{O}-\text{Au}$ bond lengths of 2.048 and 2.051 Å on the square fcc(100)-like face are energetically the most stable (**Figure 4** and **Table 2**).

In addition to elucidating the mechanism of the C_2H_4 oxidation process, the coadsorption of $\text{C}_2\text{H}_4 + \text{O}_2$ was also discussed. The optimized geometries and coadsorption energies are displayed in **Figure 5** and **Table 3**, respectively. Seven configurations of the square fcc(100)-like face and nine configurations of the hexagonal fcc(111)-like face were found as shown in **Figure 5**. Their adsorption energies are within -0.63 to -1.68 eV. Interestingly, three of them ($\text{O}_2\text{-T}_3\text{-}\eta^1$, $\text{O}_2\text{-T}_1\text{-}\eta^1\text{-C}_2\text{H}_4\text{-T}_1\text{-}\eta^1$, and $\text{O}_2\text{-T}_2\text{-}\eta^1\text{-C}_2\text{H}_4\text{-T}_1\text{-}\eta^1$) react to form OMME-like species (CCOO). The calculated adsorption energies of $\text{O}_2\text{-T}_3\text{-}\eta^1\text{-C}_2\text{H}_4\text{-T}_3\text{-}\eta^1$, $\text{O}_2\text{-T}_1\text{-}\eta^1\text{-C}_2\text{H}_4\text{-T}_1\text{-}\eta^1$, and $\text{O}_2\text{-T}_2\text{-}\eta^1\text{-C}_2\text{H}_4\text{-T}_1\text{-}\eta^1$ species are -1.64, -1.67, and -1.48 eV, respectively (**Table 3**). The OMME-like intermediate would be the vital precursor state for epoxide formation and would exist at the Au/support interface during the epoxidation process.

Reaction Mechanisms of C_2H_4 with O_2 on the Au_{38} Nanocluster. As shown in **Figure 1**, the structure of the O_h -symmetric Au_{38} nanocluster has six equivalent square fcc(100)-

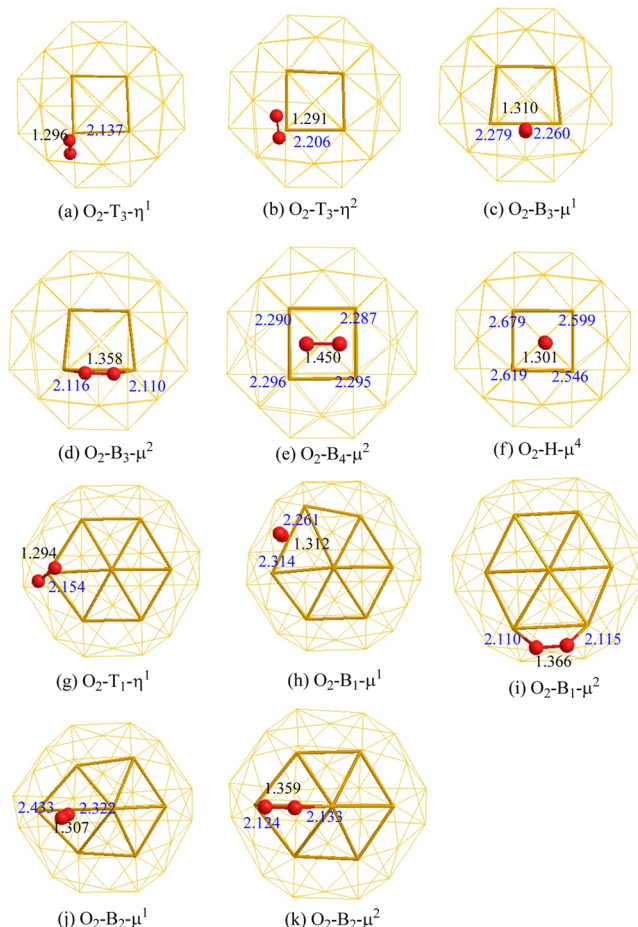


Figure 3. Optimized isomers of adsorbed O_2 on the Au_{38} nanocluster and their important geometric parameters computed at the PW91 level of theory. The bond lengths are given in angstroms.

like faces and eight equivalent hexagonal fcc(111)-like faces. Therefore, we explore the reaction mechanisms of C_2H_4 with O_2 on both the square fcc(100)-like face and the hexagonal

Table 2. Calculated Adsorption Energies (eV) and Geometrical Parameters (\AA) of Adsorbed O_2 and O on the Au_{38} nanocluster

O_2 species	E_{ads} (eV)	$d_{\text{Au1-O1}}(\text{\AA})$	$d_{\text{O1-O2}}(\text{\AA})$	$d_{\text{O2-Au2}}(\text{\AA})$
$\text{O}_2\text{-T}_3\text{-}\eta^1$	-0.16	2.137	1.296	
$\text{O}_2\text{-T}_3\text{-}\eta^2$	-0.44	2.206	1.291	3.733
$\text{O}_2\text{-B}_3\text{-}\mu^1$	-0.30	2.260, 2.279	1.310	
$\text{O}_2\text{-B}_3\text{-}\mu^2$	-0.99	2.116	1.358	2.110
$\text{O}_2\text{-B}_4\text{-}\mu^2$	-0.96	2.287, 2.295	1.450	2.290, 2.96
$\text{O}_2\text{-H-}\mu^4$	-0.32	2.619, 2.546, 2.599, 2.679	1.301	
$\text{O}_2\text{-T}_1\text{-}\eta^1$	-0.15	2.133	1.298	
$\text{O}_2\text{-B}_1\text{-}\mu^1$	-0.35	2.261, 2.314	1.312	
$\text{O}_2\text{-B}_1\text{-}\mu^2$	-0.98	2.110	1.366	2.12
$\text{O}_2\text{-B}_2\text{-}\mu^1$	-0.25	2.433, 2.322	1.307	
$\text{O}_2\text{-B}_2\text{-}\mu^2$	-0.74	2.133	1.359	2.124
O species	E_{ads} (eV)	$d_{\text{Au1-O}}(\text{\AA})$		
$\text{O-T}_3\text{-}\eta^1$	-2.75	1.895		
$\text{O-B}_3\text{-}\mu^1$	-3.72	2.048, 2.051		
$\text{O-H-}\mu^4$	-3.68	2.305, 2.336, 2.331, 2.298		
$\text{O-h-}\mu^3$	-3.93	2.156, 2.160, 2.149		

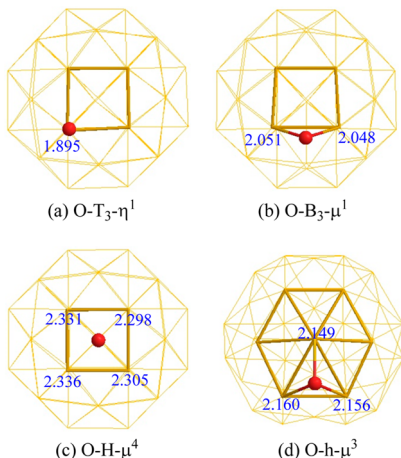
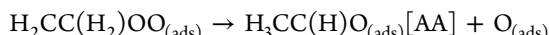
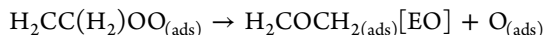
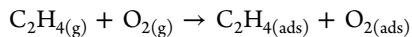


Figure 4. Optimized isomers of adsorbed O on the Au_{38} nanocluster and their important geometric parameters computed at the PW91 level of theory. The bond lengths are given in angstroms.

fcc(111)-like face. The possible reaction mechanisms with the minimum-energy barriers are proposed, including the following steps:



The potential energy surfaces (PES) of the C_2H_4 with O_2 reaction on the square fcc(111)-like face and hexagonal fcc(100)-like face were mapped in Figures 6 and 7 by using the NEB method. The predicted geometries of transition states of the reaction are presented in Figure 8.

On the hexagonal fcc(111)-like face, the reaction can start from the $\text{C}_2\text{H}_4(\text{ads})$ or $\text{O}_2(\text{ads})$ adsorption with adsorption energies of -0.53 and -0.98 eV, respectively. Then, $\text{C}_2\text{H}_4(\text{ads})$ and $\text{O}_2(\text{ads})$ are coadsorbed to form the $\text{C}_2\text{H}_4(\text{ads}) + \text{O}_2(\text{ads})$

intermediate ($\text{O}_2\text{-B}_1\text{-}\mu^2\text{-C}_2\text{H}_4\text{-B}_1\text{-}\mu^2$) with an exothermicity of 1.53 eV which is slightly larger than the sum of the adsorption energies of $\text{C}_2\text{H}_4(\text{ads})$ and $\text{O}_2(\text{ads})$ (-1.51 eV). In coadsorbed $\text{C}_2\text{H}_4(\text{ads}) + \text{O}_2(\text{ads})$ species, both $\text{C}_2\text{H}_4(\text{ads})$ and $\text{O}_2(\text{ads})$ bidentately adsorbed on two Au atoms, forming two C–Au bonds (2.180 and 2.189 Å) and two O–Au bonds (2.167 and 2.169 Å) (Figure 5). Instead of the O–O bond dissociation of O_2 (the barrier is calculated to be 1.55 eV), coadsorbed $\text{C}_2\text{H}_4(\text{ads})$ and $\text{O}_2(\text{ads})$ in the $\text{O}_2\text{-B}_1\text{-}\mu^2\text{-C}_2\text{H}_4\text{-B}_1\text{-}\mu^2$ can approach each other and bind through the oxygen atom of $\text{O}_2(\text{ads})$ to the adsorbed $\text{C}_2\text{H}_4(\text{ads})$ via TS1 ($E_a = 1.05$ eV), forming an oxometallacycle-type intermediate (OMME; $\text{O}_2\text{-T}_1\text{-}\eta^1\text{-C}_2\text{H}_4\text{-T}_1\text{-}\eta^1$), which is 1.67 eV lower than the reactants. The forming bond of C–O in TS1 is computed to be 2.392 Å, which is 0.974 Å longer than that in $\text{O}_2\text{-T}_1\text{-}\eta^1\text{-C}_2\text{H}_4\text{-T}_1\text{-}\eta^1$. As depicted in Figure 6, two reaction pathways starting from the OMME intermediate are considered: epoxide and acetaldehyde formation. The epoxide formation is calculated to be exothermic by 0.73 eV with a barrier of 1.09 eV by passing TS2, whereas the acetaldehyde formation is more exothermic by 1.36 eV but requires a higher barrier (1.28 eV) to overcome TS3. In TS2, the broken O–O bond and forming C–O bond are predicted to be 2.882 and 2.491 Å, respectively. The broken O–O bond and forming C–H bond are calculated to be 2.367 and 1.527 Å in TS3. To recapitulate, the overall epoxide formation reaction $\text{C}_2\text{H}_4(\text{g}) + \text{O}_2(\text{g}) \rightarrow \text{C}_2\text{H}_4(\text{ads}) + \text{O}_2(\text{ads}) \rightarrow \text{TS1} \rightarrow \text{H}_2\text{CC}(\text{H}_2)\text{OO}_{(\text{ads})}$ [OMME] $\rightarrow \text{TS2} \rightarrow \text{O}_{(\text{ads})} + \text{epoxide}_{(\text{gas})}$ has an exothermicity of 2.40 eV without any intrinsic barrier because the calculated energies of all of the intermediates and transition states (TS1 and TS2) are below the reactants. For the acetaldehyde formation reaction, it proceeds by $\text{C}_2\text{H}_4(\text{g}) + \text{O}_2(\text{g}) \rightarrow \text{C}_2\text{H}_4(\text{ads}) + \text{O}_2(\text{ads}) \rightarrow \text{TS1} \rightarrow \text{H}_2\text{CC}(\text{H}_2)\text{OO}_{(\text{ads})}$ [OMME] $\rightarrow \text{TS3} \rightarrow \text{O}_{(\text{ads})} + \text{acetaldehyde}_{(\text{gas})}$ with an overall reaction exothermicity of 3.03 eV without any intrinsic barrier. The calculations show that the epoxide formation reaction is substantially favored on the hexagonal fcc(111)-like face of the Au_{38} nanocluster as compared to the acetaldehyde formation reaction.

Similar to the hexagonal fcc(111)-like face, either the C_2H_4 or O_2 molecule first adsorbed on the square fcc(100)-like face with adsorption energies of -0.65 and -0.99 eV, respectively. Second, $\text{C}_2\text{H}_4(\text{ads})$ and $\text{O}_2(\text{ads})$ are coadsorbed to form the $\text{C}_2\text{H}_4(\text{ads}) + \text{O}_2(\text{ads})$ intermediate ($\text{O}_2\text{-B}_3\text{-}\mu^2\text{-C}_2\text{H}_4\text{-T}_3\text{-}\eta^2$) with an exothermicity of 1.68 eV, which is 0.04 eV larger than the sum of the adsorption energies of $\text{C}_2\text{H}_4(\text{ads})$ and $\text{O}_2(\text{ads})$ (-1.64 eV). In $\text{O}_2\text{-B}_3\text{-}\mu^2\text{-C}_2\text{H}_4\text{-T}_3\text{-}\eta^2$, $\text{C}_2\text{H}_4(\text{ads})$ is bridged at one Au atom while $\text{O}_2(\text{ads})$ is bidentately adsorbed on two Au atoms as illustrated in Figure 5. The two forming C–Au bonds of $\text{C}_2\text{H}_4(\text{ads})$ are calculated to be 2.311 and 2.313 Å, and the two O–Au bonds of $\text{O}_2(\text{ads})$ are predicted to be 2.107 and 2.114 Å. $\text{C}_2\text{H}_4(\text{ads})$ and $\text{O}_2(\text{ads})$ in $\text{O}_2\text{-B}_3\text{-}\mu^2\text{-C}_2\text{H}_4\text{-T}_3\text{-}\eta^2$ each react to form a oxometallacycle-type intermediate (OMME, $\text{O}_2\text{-T}_3\text{-}\eta^1\text{-C}_2\text{H}_4\text{-T}_3\text{-}\eta^1$) which is 0.04 eV slightly higher than the $\text{O}_2\text{-B}_3\text{-}\mu^2\text{-C}_2\text{H}_4\text{-T}_3\text{-}\eta^2$ intermediate in energy by passing TS4. The barrier is calculated to be 0.70 eV, which is 0.35 eV smaller than that in the case of the hexagonal fcc(111)-like face. As shown in Figure 7, the epoxide formation from the OMME intermediate, $\text{O}_2\text{-T}_3\text{-}\eta^1\text{-C}_2\text{H}_4\text{-T}_3\text{-}\eta^1$, is calculated to be exothermic by 0.56 eV with a lower barrier of 0.78 eV by passing TS5, whereas acetaldehyde formation is more exothermic by 1.44 eV but requires a much high barrier (1.23 eV) to overcome TS6. The epoxide formation reaction is also favored on the square fcc(100)-like face of the Au_{38} nanocluster. Compared to the case of the

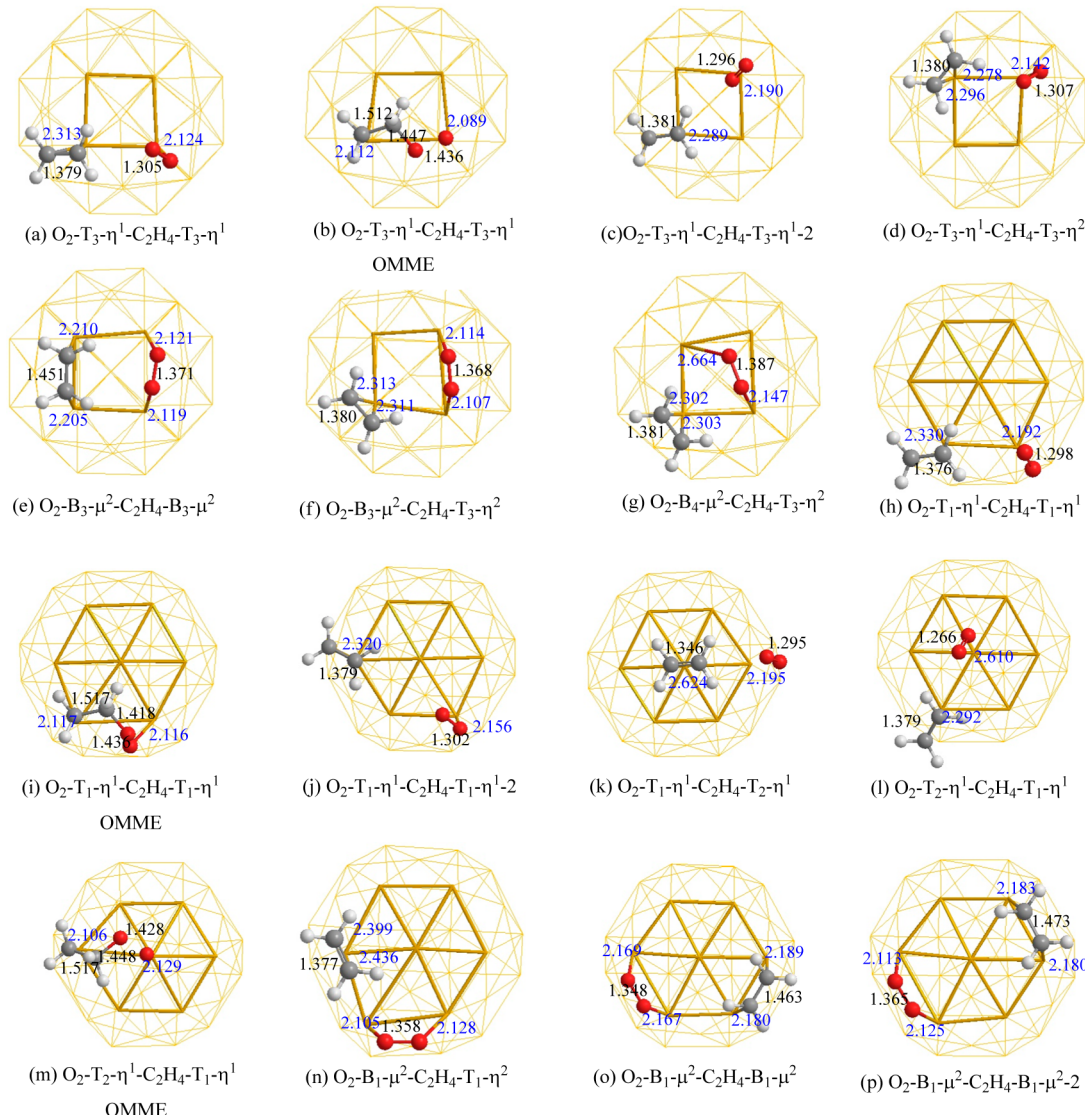


Figure 5. Optimized isomers of coadsorbed C_2H_4 and O_2 species on Au_{38} nanocluster and their important geometrical parameters computed at the PW91 level of theory. The bond lengths are given in angstroms.

Table 3. Calculated Adsorption Energies (eV) and Geometrical Parameters (\AA) of Coadsorbed $C_2H_4\text{-O}_2$ on the Au_{38} Nanocluster

species	E_{ads} (eV)	$d_{\text{Au1-O1}}(\text{\AA})$	$d_{\text{O1-O2}}(\text{\AA})$	$d_{\text{O2-C1}}(\text{\AA})$	$d_{\text{C1-C2}}(\text{\AA})$	$d_{\text{C2-Au2}}(\text{\AA})$
$O_2\text{-T}_3\text{-}\eta^1\text{-C}_2\text{H}_4\text{-T}_3\text{-}\eta^1$	-0.97	2.124	1.305	3.171	1.379	2.313
$O_2\text{-T}_3\text{-}\eta^1\text{-C}_2\text{H}_4\text{-T}_3\text{-}\eta^1$ (OMME)	-1.64	2.089	1.436	1.447	1.512	2.112
$O_2\text{-T}_3\text{-}\eta^1\text{-C}_2\text{H}_4\text{-T}_3\text{-}\eta^1\text{-}2$	-0.71	2.190	1.296	3.440	1.381	2.289
$O_2\text{-T}_3\text{-}\eta^1\text{-C}_2\text{H}_4\text{-T}_3\text{-}\eta^2$	-1.02	2.142	1.307	3.205	1.380	2.296
$O_2\text{-B}_3\text{-}\mu^2\text{-C}_2\text{H}_4\text{-B}_3\text{-}\mu^2$	-1.48	2.119, 2.121	1.371	3.555, 3.724	1.451	2.210, 2.205
$O_2\text{-B}_3\text{-}\mu^2\text{-C}_2\text{H}_4\text{-T}_3\text{-}\eta^2$	-1.68	2.107, 2.114	1.368	3.580	1.380	2.311, 2.313
$O_2\text{-B}_4\text{-}\mu^2\text{-C}_2\text{H}_4\text{-T}_3\text{-}\eta^2$	-1.58	2.147, 2.201	1.387	3.502	1.381	2.303, 2.302
$O_2\text{-T}_1\text{-}\eta^1\text{-C}_2\text{H}_4\text{-T}_1\text{-}\eta^1$	-1.11	2.192	1.298	3.369	1.376	2.330
$O_2\text{-T}_1\text{-}\eta^1\text{-C}_2\text{H}_4\text{-T}_1\text{-}\eta^1$ (OMME)	-1.67	2.116	1.436	1.418	1.517	2.117
$O_2\text{-T}_1\text{-}\eta^1\text{-C}_2\text{H}_4\text{-T}_1\text{-}\eta^1\text{-}2$	-0.76	2.156	1.302	4.628	1.379	2.320
$O_2\text{-T}_1\text{-}\eta^1\text{-C}_2\text{H}_4\text{-T}_2\text{-}\eta^1$	-0.63	2.195	1.295	3.097	1.346	2.624
$O_2\text{-T}_2\text{-}\eta^1\text{-C}_2\text{H}_4\text{-T}_1\text{-}\eta^1$	-0.85	2.610	1.266	3.283	1.379	2.292
$O_2\text{-T}_2\text{-}\eta^1\text{-C}_2\text{H}_4\text{-T}_1\text{-}\eta^1$ (OMME)	-1.48	2.129	1.428	1.448	1.517	2.106
$O_2\text{-B}_1\text{-}\mu^2\text{-C}_2\text{H}_4\text{-T}_1\text{-}\eta^2$	-1.29	2.128, 2.105	1.358	3.249	1.377	2.399, 2.436
$O_2\text{-B}_1\text{-}\mu^2\text{-C}_2\text{H}_4\text{-B}_1\text{-}\mu^2$	-1.53	2.169	1.348	4.757	1.463	2.189
$O_2\text{-B}_1\text{-}\mu^2\text{-C}_2\text{H}_4\text{-B}_1\text{-}\mu^2\text{-}2$	-1.44	2.113	1.365	5.996	1.473	2.183

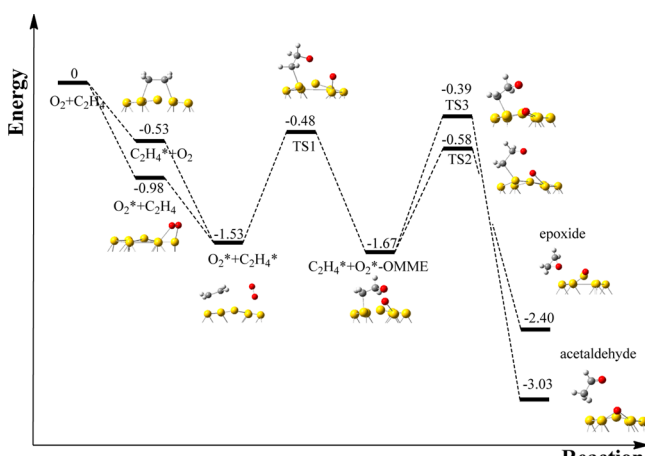


Figure 6. Calculated potential energy surface for the reaction of C_2H_4 and O_2 on the hexagonal fcc(111)-like face of the Au_{38} nanocluster. All energies (eV) are related to the isolated reactants.

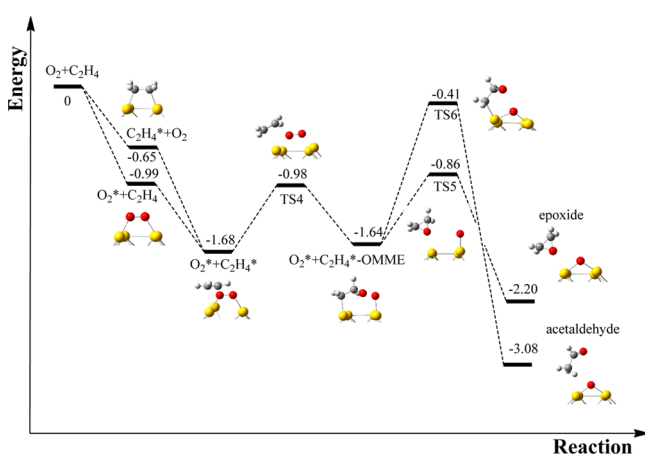


Figure 7. Calculated potential energy surface for the reaction of C_2H_4 and O_2 on the square fcc(100)-like face of the Au_{38} nanocluster. All energies (eV) are related to the isolated reactants.

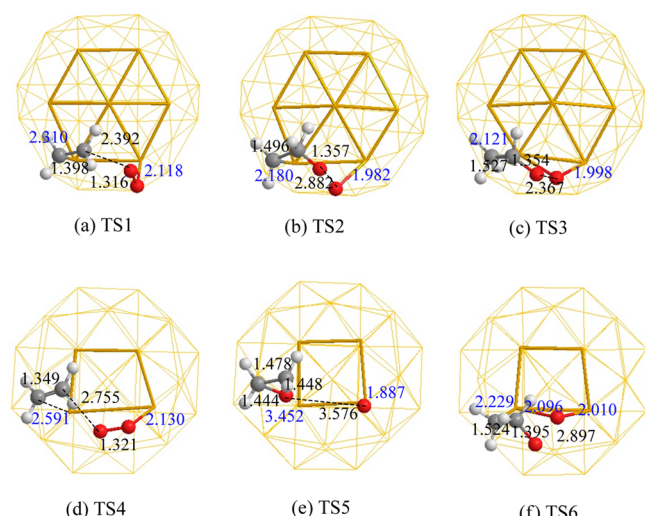


Figure 8. Geometrical illustration of transition states for the reactions on the hexagonal fcc(111)-like face and the square fcc(100)-like face of the Au_{38} nanocluster. The bond lengths are given in angstroms.

hexagonal fcc(111)-like face, the square fcc(100)-like face active site exhibits higher catalytic activity for the formation of the C–O bond and the breaking of the O–O bond in the epoxide formation reaction because of lower barriers (**Figures 6** and **7**). An increase in epoxide selectivity on the square fcc(100)-like face is found due to changes in the activation barrier of epoxide formation and acetaldehyde formation from the OMME intermediate. The activation barrier of epoxide formation is computed to be lower than the activation barrier of acetaldehyde formation by 0.45 eV for the square fcc(100)-like face and lower by 0.19 eV for the hexagonal fcc(111)-like face.

Analysis of the Electronic State During Ethylene Oxidation Reaction. The calculated electronic local density of states (LDOS) of the system projected onto the orbitals for the O_2 species (left panel) and the C_2H_4 species (right panel) and the d -projected electron density of the Au atoms (four and seven Au atoms are chosen for the square fcc(100)-like face and hexagonal fcc(111)-like face, respectively) are plotted in **Figure 9** and **Figure S3**. The a and g in **Figure 9** display the LDOS before the interaction between the O_2 (C_2H_4) and the square fcc(100)-like face of the Au_{38} nanoparticle; **Figure 8b(h)–f(l)** corresponds to the LDOS of $O_{2(ads)}$ [$C_{2H_4(ads)}$], $O_{2(ads)} + C_{2H_4(ads)}$, OMME, epoxide, and acetaldehyde configurations, respectively. There is a broad overlap between the O_2 p and Au d orbitals over 2.0 to –9.0 eV for the O_2 species on the nanoparticle (**Figure 8b**). The electronic states (C_2H_4 s, C_2H_4 p, and Au d states) coupling between the C_2H_4 and the nanoparticle are found to be in the range of 1.0 to –8.0 eV for the C_2H_4 species on the nanoparticle (**Figures 8h**). The results indicate the stronger interaction between the molecules of adsorbate and the substrate. The LDOS (**Figure 8c,i**) of $O_{2(ads)} + C_{2H_4(ads)}$ is similar to $O_{2(ads)}$ or $C_{2H_4(ads)}$. As the oxidation proceeds, it can be seen that, from $O_{2(ads)} + C_{2H_4(ads)}$ to OMME, orbitals (the O_2 p, C_2H_4 s, C_2H_4 p and Au d states, **Figure 8d,j**) apparently show stronger and broader hybridization between the O_2 (O_2 p state) or C_2H_4 (C_2H_4 s and C_2H_4 p states) and the Au atoms (d orbital). Because of the formation of C–O bond in OMME, further interaction between O_2 (O_2 p state) and C_2H_4 (C_2H_4 s and C_2H_4 p states) species is clearly observed in the range of 0.0 to –8.0 eV, as shown in **Figure 8d,j**. Finally, in **Figure 8e,f,k,l**, the LDOS for the reaction products are combined with the LDOS of the adsorbed epoxide, acetaldehyde, and O adsorbates on the Au_{38} nanoparticle. In addition, we carried out the DOS calculations for both the Au_{38} nanocluster and $Au(111)$ surface as depicted in **Figure S4**. The molecules (C_2H_4 or O_2) are adsorbed more favorably on the Au_{38} nanocluster than on the $Au(111)$ surface because of the higher-lying d-state contribution.

CONCLUSIONS

The adsorption behavior of C_2H_4 and O_2 on the Au_{38} nanoparticle and their electronic properties and the oxidation reaction mechanisms have been studied by spin-polarized DFT calculations. According to our calculation results, the C_2H_4 – T_1 – η^2 , O_2 – B_3 – μ^2 , and O – h – μ^3 adsorptions are energetically favored among all predicted configurations of C_2H_4/Au_{38} , O_2/Au_{38} , and O/Au_{38} . Potential energy surfaces for the $C_2H_4 + O_2$ reaction on the Au_{38} nanoparticle have been illustrated by employing the NEB method. The overall reaction of $C_2H_4 + O_2 + Au_{38} \rightarrow$ ethylene oxide + O/Au_{38} is exothermic by 2.40 eV on the hexagonal fcc(111)-like face and 2.20 eV on the square fcc(100)-like face whereas those are 3.03 and 3.08 eV for the production of acetaldehyde and O/Au_{38} . The calculations show

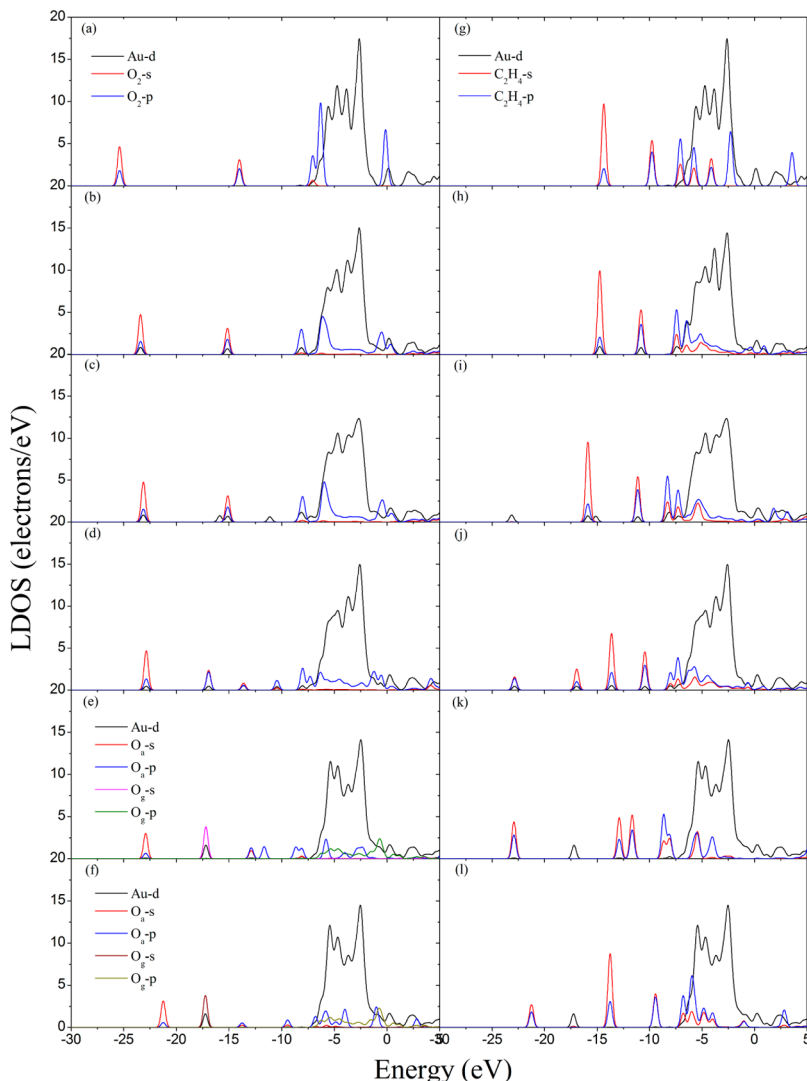


Figure 9. Calculated electronic local density of states (LDOS) of the system projected on the orbitals for the adsorbed constructs of O_2 (left panel) and C_2H_4 (right panel) species as well as the d projection of the Au atoms on the square fcc(100)-like face. O_a and O_g represent the remaining oxygen atom adsorbed on the nanocluster and the oxygen atom of epoxide or acetaldehyde.

that the epoxide formation reaction is substantially favored on the Au_{38} nanocluster as compared to the acetaldehyde formation reaction. Compared to the hexagonal fcc(111)-like face, the square fcc(100)-like face reveals more reactive and higher epoxide selectivity because of the lower barriers. The DFT calculations provide information on the reaction mechanism and the catalytic activity of the Au nanoparticle which would be difficultly to measure in the experiment, indicating that the periodic DFT calculations might play a significant role in such heterogeneous catalysis.

ASSOCIATED CONTENT

Supporting Information

Calculated adsorption energies and geometrical parameters of weakly adsorbed C_2H_4 on the Au_{38} nanocluster and weakly adsorbed O_2 on the Au_{38} nanocluster. Calculated weakly bound intermediates of C_2H_4 adsorbed on the Au_{38} nanocluster and O_2 adsorbed on the Au_{38} nanocluster. Calculated electronic local density of states of the system projected on the orbitals for the adsorbed constructs of O_2 and C_2H_4 species, as well as the d projection of the Au atoms on the hexagonal fcc(111)-like face. Electronic local density of states of the system projected

on the d states of the Au_{38} nanoparticle and $Au(111)$ surface. The Supporting Information is available free of charge on the ACS Publications website at DOI: [10.1021/acs.jpca.5b04737](https://doi.org/10.1021/acs.jpca.5b04737).

AUTHOR INFORMATION

Corresponding Author

*E-mail: htchen@cycu.edu.tw. Tel: +886-3-265-3324.

Notes

The authors declare no competing financial interest.

ACKNOWLEDGMENTS

We are grateful to the Ministry of Science and Technology (MOST), Taiwan, under grant numbers MOST 104-2113-M-033-010 and MOST 103-2632-M-033-001-MY3, for financial support, and the National Center for High-performance Computing, Taiwan, for the computer time and facilities.

REFERENCES

- Chen, H.-T.; Chang, J.-G.; Ju, S.-P.; Chen, H.-L. First-Principle Calculations on CO Oxidation Catalyzed by a Gold Nanoparticle. *J. Comput. Chem.* **2010**, *31*, 258–265.

- (2) Haruta, M.; Yamada, N.; Kobayashi, T.; Iijima, S. Gold Catalysts Prepared by Coprecipitation for Low-Temperature Oxidation of Hydrogen and of Carbon Monoxide. *J. Catal.* **1989**, *115*, 301–309.
- (3) Chen, H.-L.; Su, C.-H.; Chen, H.-T. Catalytic CO Oxidation by Au-Pd Core-Shell Nanoparticles: A First-Principles Study. *Chem. Phys. Lett.* **2012**, *536*, 100–103.
- (4) Bailie, J. E.; Hutchings, G. Promotion by Sulfur of Gold Catalysts for Crotyl Alcohol Formation from Crotonaldehyde Hydrogenation. *Chem. Commun.* **1999**, 2151–2152.
- (5) Landon, P.; Collier, P. J.; Papworth, A. J.; Kiely, C. J.; Hutchings, G. Direct Formation of Hydrogen Peroxide from H_2/O_2 Using a Gold Catalyst. *Chem. Commun.* **2002**, 2058–2059.
- (6) Fu, Q.; Saltsburg, H.; Flytzani-Stephanopoulos, M. Active Nonmetallic Au and Pt Species on Ceria-Based Water-Gas Shift Catalysts. *Science* **2003**, *301*, 935–938.
- (7) Lin, R.-J.; Chen, H.-L.; Ju, S.-P.; Li, F.-Y.; Chen, H.-T. Quantum-Chemical Calculations on the Mechanism of the Water-Gas Shift Reaction on Nanosized Gold Cluster. *J. Phys. Chem. C* **2012**, *116*, 336–342.
- (8) Hughes, M. D.; Xu, Y.; Jenkins, P.; McMorn, P.; Landon, P.; Enache, D. I.; Carley, A. F.; Attard, G. A.; Hutchings, G. J.; King, F.; Stitt, E. H.; Johnston, P.; Griffin, K.; Kiely, C. J. Tunable Gold Catalysts for Selective Hydrocarbon Oxidation under Mild Conditions. *Nature* **2005**, *437*, 1132–1135.
- (9) Haruta, M. Size- and Support-Dependency in the Catalysis of Gold. *Catal. Today* **1997**, *36*, 153–166.
- (10) Haruta, M. Catalysis: Gold Rush. *Nature* **2005**, *437*, 1098–1099.
- (11) Haruta, M.; Kobayashi, T.; Sano, H.; Yamada, N. Novel Gold Catalysts for the Oxidation of Carbon Monoxide at a Temperature far Below 0°C. *Chem. Lett.* **1987**, *16*, 405–408.
- (12) Turner, M.; Golovko, V. B.; Vaughan, O. P. H.; Abdulkin, P.; Berenguer-Murcia, A.; Tikhov, M. S.; Johnson, B. F. G.; Lambert, R. M. Selective Oxidation with Dioxygen by Gold Nanoparticle Catalysts Derived from 55-Atom Clusters. *Nature* **2008**, *454*, 981–983.
- (13) Valden, M.; Lai, X.; Goodman, D. W. Onset of Catalytic Activity of Gold Clusters on Titania with the Appearance of Nonmetallic Properties. *Science* **1998**, *281*, 1647–1650.
- (14) Chen, M.; Goodman, D. W. Catalytically Active Gold: From Nanoparticles to Ultrathin Films. *Acc. Chem. Res.* **2006**, *39*, 739–746.
- (15) Hashmi, A. S. K.; Hutchings, G. J. Gold Catalysis. *Angew. Chem., Int. Ed.* **2006**, *45*, 7896–7936.
- (16) Hutchings, G. J.; Burst, M.; Schmidbaur, H. Gold—an Introductory Perspective. *Chem. Soc. Rev.* **2008**, *37*, 1759–1765.
- (17) Fukuoka, A.; Dhepe, P. L. Sustainable Green Catalysis by Supported Metal Nanoparticles. *Chem. Rec.* **2009**, *9*, 224–235.
- (18) Carrettin, S.; Concepción, P.; Corma, A.; Nieto, J. M. L.; Puntes, V. F. A. Nanocrystalline CeO_2 Increases the Activity of Au for CO Oxidation by Two Orders of Magnitude. *Angew. Chem., Int. Ed.* **2004**, *43*, 2538–2540.
- (19) Gluhoi, A. C.; Dekkers, M. A. P.; Nieuwenhuys, B. E. Comparative Studies of the N_2O/H_2 , N_2O/CO , H_2/O_2 and CO/O_2 Reactions on Supported Gold Catalysts: Effect of the Addition of Various Oxides. *J. Catal.* **2003**, *219*, 197–205.
- (20) Grisel, R. J. H.; Nieuwenhuys, B. E. Selective Oxidation of CO, over Supported Au Catalysts. *J. Catal.* **2001**, *199*, 48–59.
- (21) Romero-Sarria, F.; Martinez, L. M.; Centeno, M. A.; Odriozola, J. A. Surface Dynamics of Au/CeO₂ Catalysts during CO Oxidation. *J. Phys. Chem. C* **2007**, *111*, 14469–14475.
- (22) Sanchez, A.; Abbet, S.; Heiz, U.; Schneider, W.-D.; Häkkinen, H.; Barnett, R. W.; Landman, U. When Gold Is Not Noble: Nanoscale Gold Catalysts. *J. Phys. Chem. A* **1999**, *103*, 9573–9578.
- (23) Schubert, M. M.; Hackenberg, S.; Van Veen, A. C.; Muhler, M.; Plzak, V.; Behm, R. J. CO Oxidation over Supported Gold Catalysts—“Inert” and “Active” Support Materials and Their Role for the Oxygen Supply during Reaction. *J. Catal.* **2001**, *197*, 113–122.
- (24) Haruta, M.; Tsukuda, S.; Kobayashi, T.; Kageyama, H.; Genet, M. J.; Delmon, B. CO Oxidation over Supported Gold Catalysts—“Inert” and “Active” Support Materials and Their Role for the Oxygen Supply during Reaction. *J. Catal.* **1993**, *144*, 175–192.
- (25) Liu, C.; Tan, Y.; Lin, S.; Li, H.; Wu, X.; Li, L.; Pei, Y.; Zeng, X. C. CO Self-Promoting Oxidation on Nanosized Gold Clusters: Triangular Au_3 Active Site and CO Induced O–O Scission. *J. Am. Chem. Soc.* **2013**, *135*, 2583–2595.
- (26) Chang, C. M.; Cheng, C.; Wei, C. M. CO Oxidation on Unsupported Au_{55} , Ag_{55} , and $Au_{25}Ag_{30}$ Nanoclusters. *J. Chem. Phys.* **2008**, *128*, 124710–124714.
- (27) Gao, W.; Chen, X. F.; Li, J. C.; Jiang, Q. Is Au_{55} or Au_{38} Cluster a Threshold Catalyst for Styrene Epoxidation? *J. Phys. Chem. C* **2010**, *114*, 1148–1153.
- (28) Garzón, I. L.; Michaelian, K.; Beltrán, M. R.; Posada-Amarillas, A.; Ordejón, P.; Artacho, E. Lowest Energy Structures of Gold Nanoclusters. *Phys. Rev. Lett.* **1998**, *81*, 1600–1603.
- (29) Liu, P.; Rodriguez, J. A. Water-Gas-Shift Reaction on Metal Nanoparticles and Surfaces. *J. Chem. Phys.* **2007**, *126*, 164705–164712.
- (30) Lopez, N.; Nørskov, J. K. Catalytic CO Oxidation by a Gold Nanoparticle: A Density Functional Study. *J. Am. Chem. Soc.* **2002**, *124*, 11262–11263.
- (31) Remediakis, I. N.; Lopez, N.; Nørskov, J. K. CO Oxidation on Rutile-Supported Au Nanoparticles. *Angew. Chem., Int. Ed.* **2005**, *44*, 1824–1826.
- (32) Wang, Y.; Gong, X. G. First-Principles Study of Interaction of Cluster Au_{32} with CO, H_2 , and O_2 . *J. Chem. Phys.* **2006**, *125*, 124703.
- (33) Li, H.-J.; J.-J. H. Theoretical Calculations on the Oxidation of CO on Au_{55} , $Ag_{13}Au_{42}$, $Au_{13}Ag_{42}$, and Ag_{55} Clusters of Nanometer Size. *J. Phys. Chem. C* **2012**, *116*, 13196–13201.
- (34) Patil, N. S.; Jha, R.; Uphade, B. S.; Bhargava, S. K.; Choudhary, V. R. Epoxidation of Styrene by Anhydrous t-Butyl Hydroperoxide over Gold Supported on Al_2O_3 , Ga_2O_3 , In_2O_3 and Tl_2O_3 . *Appl. Catal., A* **2004**, *275*, 87–93.
- (35) Patil, N. S.; Uphade, B. S.; McCulloh, D. G.; Bhargava, S. K.; Choudhary, V. R. Styrene Epoxidation over Gold Supported on Different Transition Metal Oxides Prepared by Homogeneous Deposition–Precipitation. *Catal. Commun.* **2004**, *5*, 681–685.
- (36) Hayashi, T.; Tanaka, K.; Haruta, M. Styrene Epoxidation over Gold Supported on Different Transition Metal Oxides Prepared by Homogeneous Deposition–Precipitation. *J. Catal.* **1998**, *178*, 566–575.
- (37) Gao, F.; Wang, Y. L.; Goodman, D. W. CO Oxidation over AuPd(100) from Ultrahigh Vacuum to Near-Atmospheric Pressures: The Critical Role of Contiguous Pd Atoms. *J. Am. Chem. Soc.* **2009**, *131*, 5734–5735.
- (38) Gao, Y.; Shao, N.; Pei, Y.; Zeng, X. C. Icosahedral Crown Gold Nanocluster $Au_{43}Cu_{12}$ with High Catalytic Activity. *Nano Lett.* **2010**, *10*, 1055–1062.
- (39) Chen, H.-T.; Chang, J.-G.; Ju, S.-P.; Chen, H.-L. Ethylene Epoxidation on a Au Nanoparticle versus a Au(111) Surface: A DFT Study. *J. Phys. Chem. Lett.* **2010**, *1*, 739–742.
- (40) Lyalin, A.; Taketsugu, T. Cooperative Adsorption of O_2 and C_2H_4 on Small Gold Clusters. *J. Phys. Chem. C* **2009**, *113*, 12930–12934.
- (41) Hohenberg, P.; Kohn, W. Inhomogeneous Electron Gas. *Phys. Rev.* **1964**, *136*, B864–B871.
- (42) Kresse, G.; Furthmüller, J. Efficient Iterative Schemes for Ab Initio Total-Energy Calculations for Metals and Semiconductors Using a Plane-Wave Basic Set. *Comput. Mater. Sci.* **1996**, *6*, 15–50.
- (43) Kresse, G.; Hafner, J. Ab Initio Molecular Dynamics for Liquid Metals. *Phys. Rev. B: Condens. Matter Mater. Phys.* **1993**, *47*, 558–561.
- (44) Kresse, G.; Hafner, J. Ab Initio Molecular-Dynamics Simulation of the Liquid-Metal–Amorphous–Semiconductor Transition in Germanium. *Phys. Rev. B: Condens. Matter Mater. Phys.* **1994**, *49*, 14251–14269.
- (45) Kresse, G.; Hafner, J. Norm-Conserving and Ultrasoft Pseudopotentials for First-Row and Transition Elements. *J. Phys.: Condens. Matter* **1994**, *6*, 8245–8257.

- (46) Kresse, G.; Hafner, J. Efficient Iterative Schemes for Ab Initio Total-Energy Calculations Using a Plane-Wave Basis Set. *Phys. Rev. B: Condens. Matter Mater. Phys.* **1996**, *54*, 11169–11186.
- (47) Perdew, J. P.; Burke, K.; Ernzerhof, M. Generalized Gradient Approximation Made Simple. *Phys. Rev. Lett.* **1996**, *77*, 3865–3868.
- (48) Perdew, J. P.; Wang, Y. Accurate and Simple Analytic Representation of the Electron-Gas Correlation Energy. *Phys. Rev. B: Condens. Matter Mater. Phys.* **1992**, *45*, 13244–13249.
- (49) Henkelman, G.; Uberuaga, B. P.; Jónsson, H. A Climbing Image Nudged Elastic Band Method for Finding Saddle Points and Minimum Energy Paths. *J. Chem. Phys.* **2000**, *113*, 9901–9904.
- (50) Mills, G.; Jónsson, H.; Schenter, G. K. Reversible Work Transition State Theory: Application to Dissociative Adsorption of Hydrogen. *Surf. Sci.* **1995**, *324*, 305–337.
- (51) Häberlen, O. D.; Chung, S.-C.; Stener, M.; Rösch, N. From Clusters to Bulk: A Relativistic Density Functional Investigation on a Series of Gold Clusters Au_n , $n=6,\dots,147$. *J. Chem. Phys.* **1997**, *106*, 5189–5201.
- (52) Lyalin, A.; Taketsugu, T. Adsorption of Ethylene on Neutral, Anionic, and Cationic Gold Clusters. *J. Phys. Chem. C* **2010**, *114*, 2484.